Surg Radiol Anat (2017) 39:367–374
DOI 10.1007/s00276-016-1743-5

ORIGINAL ARTICLE

# Volumetric study of sphenoid sinuses: anatomical analysis in helical computed tomography

**Juliana Mayara Magalhães Oliveira[1] · Maria Beatriz Carrazzone Cal Alonso[1,2] · Maria José Albuquerque Pereira de Sousa e Tucunduva[1] · Acácio Fuziy[1,2] · Ana Carla Raphaelli Nahás Scocate[1,2] · André Luiz Ferreira Costa[1,2]**

Received: 5 May 2016 / Accepted: 6 September 2016 / Published online: 15 September 2016


**Abstract**
*Purpose* The sphenoid sinus is the most inaccessible part of the face, being inside the sphenoid bone and closely related to numerous vital neural and vascular structures. The objective of this study was to analyze and evaluate the variation of anatomy and the volume of the sphenoid sinus using helical computed tomography and medical imaging software.
*Materials and methods* A total of 47 helical CT scans of sinuses of male and female individuals aged 18–86 years were selected. The images were formatted using ITK-SNAP software, consisting of three steps: (1) segmentation; (2) volumetric analysis and (3) 3D reconstruction. The sphenoid sinuses were also classified according to Hammer, i.e., in conchal, pre-sellar, sellar and post-sellar types. A single investigator, who is specialist in dental radiology and was trained and calibrated, performed the volume and image analysis. After 15 days, the segmentations were repeated.
*Results* The Dunn's multiple comparison test revealed significant differences in the volume rankings between the right and left sides ($P = 0.0002$), with the post-sellar type presenting the greatest volume on the right side compared to pre-sellar and sellar types. In the left sphenoid sinuses, the post-sellar type showed the greatest volume. The Lin's correlation coefficient showed excellent reproducibility values.
*Conclusions* According to the applied methodology, it was found that the volume of the sphenoid sinus was influenced by neither age nor gender ($P > 0.005$). There was difference in the volumes of sphenoid sinus on the right and left sides and in the anatomical classification.

**Keywords** Sphenoid sinus · Anatomy · Computed tomography

## Introduction

The sphenoid sinus is enclosed within the sphenoid body involving a number of different structures, which makes it difficult to approach it due to its deep anatomical location. They vary in shape and size and are usually asymmetric. They are surrounded by neurovascular structures such as pituitary gland, internal carotid artery, optic nerve, maxillary nerve and pterygoid nerve. Therefore, the knowledge of the anatomical variations of these noble structures is fundamental to avoid careless manipulation, which can result in very serious complications with poor prognosis.

The sphenoid sinus has the peculiarity to reflect its anatomical relationships in its walls. The surrounded structures record a mark on its internal walls when the sinus is pneumatized and expanded, increase its contacts with these structures [1, 17]. This intimate relationship contributes to the unquestionable clinical and surgical importance of the sphenoid sinus. The frequency at which such structures protrude into the sphenoid sinus is high, being increasingly necessary to stress the importance of a

✉ Maria Beatriz Carrazzone Cal Alonso
mbialonso_usp@yahoo.com.br

[1] Department of Dentistry, City of São Paulo University, UNICID, Rua Cesário Galeno 448, Bloco A. Tatuapé, São Paulo 03071-000, SP, Brazil

[2] Department of Orthodontics and Radiology, UNICID, São Paulo, Brazil

precise anatomical knowledge in the surgical and clinical practice [1, 14, 17, 23, 25, 30].

The sphenoid sinuses can be classified into apneumatized, conchal, pre-sellar, post-sellar and sellar. For pneumatization of the sphenoid sinus, the extension of pneumatization and the degree of exposure of the sella turcica should be taken into account (Hammer and Radberg classification [12], adapted by Dias et al. [9]) as follows: (1) apneumatized, i.e., sinus agenesis; (2) conchal, i.e., slightly pneumatized small sinus not related to the sella turcica; (3) pre-sellar, i.e., pneumatization does not extend beyond the vertical plane of the sellar tubercle; (4) sellar, i.e., pneumatization of the sphenoid sinus reaches the vertical plane of the posterior clinoid process, involving both anterior wall and floor of the sella turcica; and (5) post-sellar, i.e., pneumatization of the sphenoid sinus extends beyond the sella turcica, reaching the basilar part of the occipital process.

The advent of functional endoscopic sinus surgery (FESS) and modern imaging techniques has allowed the sinus to be more frequently accessed not only for treatment of diseases, but also as a path towards the pituitary gland. With regard to minimally invasive surgical approaches and advances in endoscopic techniques, the sphenoid sinus can be used as a way to reach tumors involving the anterior skull base, peri-sellar region, clivus, petroclival region and cavernous sinus [2–4].

Understanding the anatomy of the sinus area and its variations in each patient should be carefully evaluated so that the surgeon can achieve a better surgical result, thus maximizing the patient's safety as anatomical variations of sphenoid sinus and sella turcica can complicate the surgical proceedings [13, 16, 26].

Computed tomography (CT) is currently the imaging modality of choice for assessment of paranasal sinuses and adjacent structures. It has been increasingly used for evaluation of anatomical variations by identifying them accurately and with high details [2, 9, 19, 26].

The type of sinus and its basic dimensions (height, width and length) can help predict the risk of accidental injury [25]. Few studies have been conducted considering all age groups. The practical importance of the results is to classify the sphenoid sinus according to its position in the sella turcica. Understanding the normal volume of the sinus based on CT techniques will help the professional determine the pathological development of structures in an appropriate clinical context [4, 21, 28]. Since it has been reported that the 3D reconstruction of anatomical structures allows good-quality views of the components, thus being a useful method for further studies [8, 10, 27]. The aim of this study was to analyze and evaluate the anatomical variations and the volume of the sphenoid sinus by using helical CT.

## Materials and methods

This study was conducted in accordance with the universally accepted rules and precepts for research involving human subjects, being approved by the local research ethics committee of the City of São Paulo University according to Protocol Number 999206.

All helical CT scans were provided from a private diagnostic center database and were originally taken as part of previous research about paranasal sinuses performed between March 2012 and December 2012. No patient had previous sinus surgery, craniofacial trauma or pathological conditions in maxillofacial area. The total number of original scans was 89. Of these, 42 scans did not have a good image quality and/or no showed our area of interest and were excluded from the study. The images were taken with a CT scanner (Somatom AR Star/Siemens) operating at 83 mA and 110 kV. The protocol used was characterized by 2-mm axial thickness, 5-mm coronal increments, 3-mm thickness, and 3-mm increments. The slices were acquired with the patient in supine position, without introduction of contrast medium or use of decongestant medication. Coronal sections of the external frontal bone were taken perpendicularly to the bony palate, including the posterior wall of the sphenoid bone on the axial plane, limiting at the soft tissue boundary.

A total of 47 CT helical scans of 27 female and 20 male patients aged between 18 and 86 years old were selected. All scans were analyzed with the ITK/SNAP software (http://www.itksnap.org/download/snap/) [32], an open source medical image computing platform for biomedical research and which enables visualization (coronal, sagittal and horizontal orientations) and manipulation of the images as it can optimize them through reconstruction plans [29]. This software allows manual and semi-automatic segmentation and the choice of different colors for the structures outlined. In the segmentation, the similarity in gray levels between tissues of same density allows the localization of image edges and, consequently, the total mapping of the structure studied. Volumes of labeled structures are analyzed automatically by the software. Regions of interest can be edited manually and semiautomatically by thresholding the image. The program also allows 3D surface rendering and interactive manipulation [5, 6, 8, 29].

A single investigator, who is a dentomaxillofacial radiologist, trained and calibrated, performed the image segmentation by measuring the volume and shape of the sphenoid sinus. Points were selected to produce a visually appropriate layout of the surface of the sinus contour following carefully its anatomical borders. For visualization and delineation, the axial section was selected (Fig. 1) and complemented sagittally and coronally. After complete segmentation of the sinus, ITK/SNAP software was used to calculate the total volume of the structure in $mm^3$. Additionally, we reconstructed the sinus

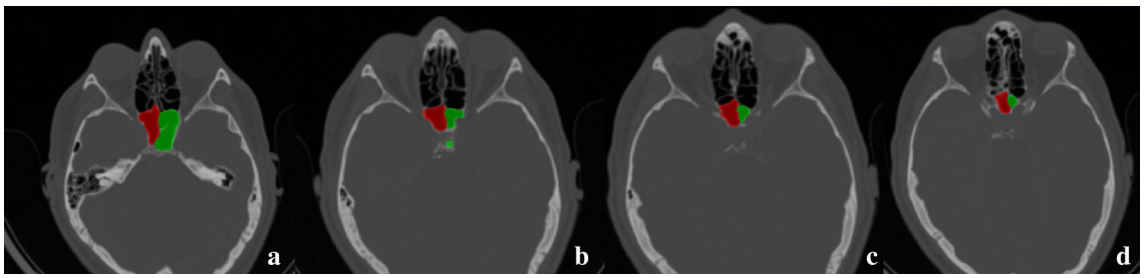


**Fig. 1** Series **a–d** of images exemplifying the segmentation for *each image* slice in the *axial section* (ITK/SNAP)

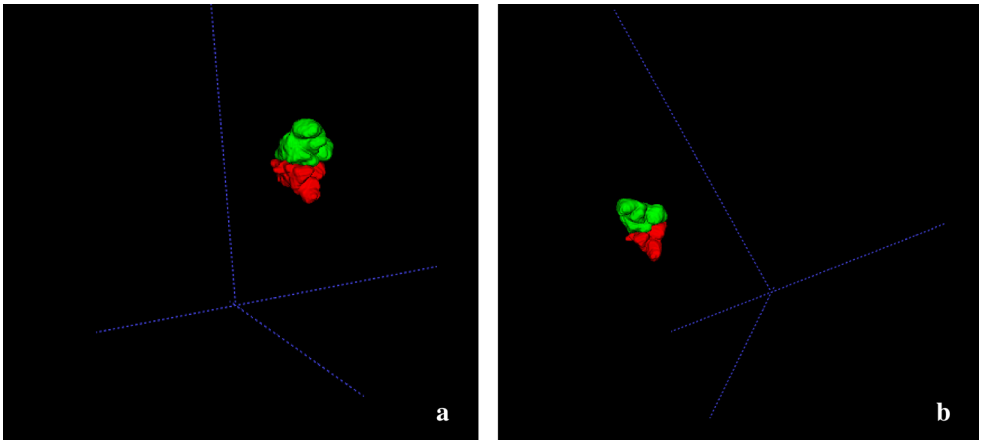


**Fig. 2** Series **a**, **b** of images exemplifying the 3D reconstruction of the sinus (ITK/SNAP)

three-dimensional (3D), which allowed to compare the anatomical classification to that of the literature (Fig. 2). After a period of 15 days, the same procedures were repeated for analysis of the intra-rater agreement. The sphenoid sinuses were classified according to Hammer and Radberg [12] adapted by Dias et al. [9], in nonpneumatized, conchal, pre-sellar, sellar and post-sellar.

### Statistical analysis

All the information obtained was analyzed by using the SAS 9.4 and Minitab 16 statistical software. The Lin's concordance correlation coefficient and limit-of-agreement (Bland and Altman) were used to assess the agreement between the repetitions. Both volume comparison between genders and classification were performed using the Mann–Whitney test. The correlation between volume and age was assessed using the Spearman's coefficient. The confidence level used in the analysis was 95 %.

## Results

Table 1 shows that both right and left sides of the first measurement were slightly smaller than those of the second measurement, with a significant difference between both sides. However, the Lin's correlation coefficient (CC) is very close to 1, indicating an almost perfect agreement between the two measurements. This high correlation can also be seen in the left graph of Figs. 3 and 4. In the right graph, one can observe that both measurements are similar, since the observations do not follow any pattern and a few points (less than expected) are out of the bounds. As the magnitude of the bias is close to the magnitude of the measurements, it can be inferred that this difference is not significant in the practice, despite being statistically significant. Given the high correlation between the two measurements, the following analysis was used to find the average of both measurements for the volume (Fig. 5).

Table 2 shows that significant differences were found between the volume rankings on the right side ($P$ value = 0.0002). The Dunn's multiple comparison test showed that post-sellar category had a higher volume than the pre-sellar and sellar categories.

Table 3 shows that significant differences were found between the volume rankings on the left side ($P$ value = 0.0002). The nonpneumatized, or sinus agenesis, was not seen in our study. Post-sellar category showed a higher volume than the sellar category. In Table 4, it is noted that there is no linear correlation between volume and age. No meaningful correlations were identified between age, gender and volume sphenoid sinus according to the Spearman correlation analysis.

**Table 1** Analysis agreement between the measurements

| Side | First measure | | Second measure | | Bias | *P* value | IC bias | CC |
|---|---|---|---|---|---|---|---|---|
| | Average | ±SD | Average | SD | | | | |
| Right | 6031.98 | 3488.65 | 6157.37 | 3495.40 | −125.39 | <0.001 | (−174.91; −75.88) | 0.998 |
| Left | 7178.68 | 3571.28 | 7256.87 | 3588.35 | −78.19 | 0.011 | (−482.66; 326.28) | 0.998 |

Volumes (mm3)

*SD* standard deviation

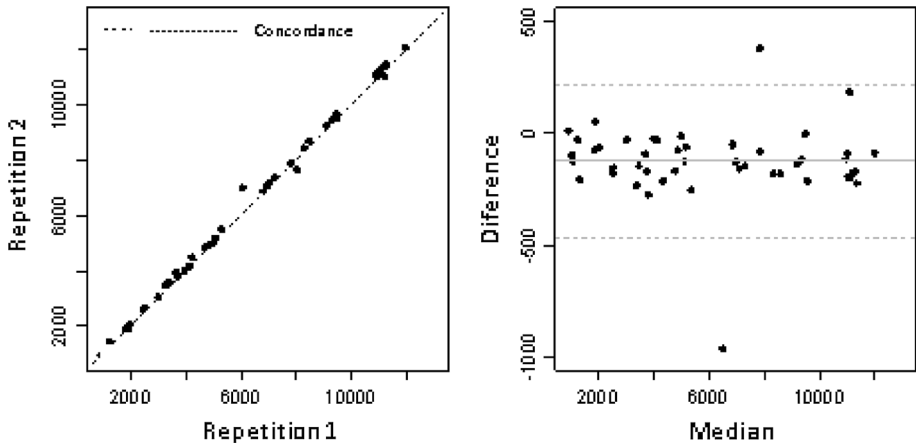


**Fig. 3** *Scatter plots* and Bland and Altman plots for the volume on the *right side*

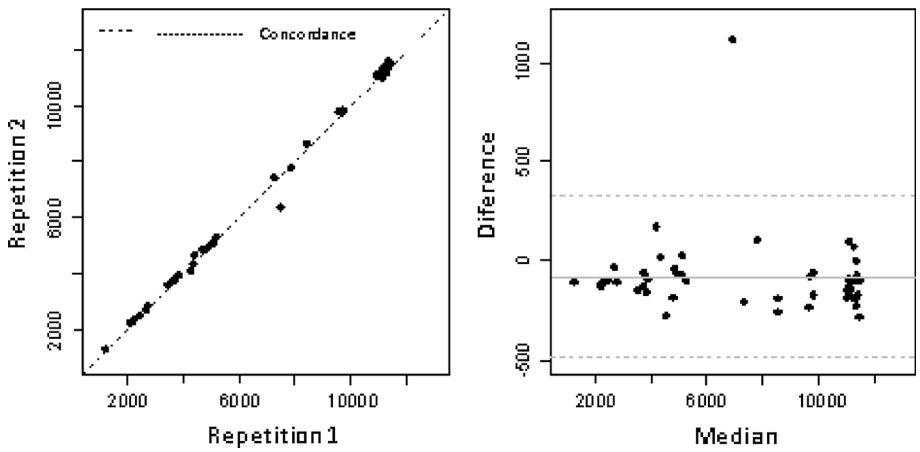


**Fig. 4** *Scatter plots* and Bland and Altman to the volume of the *left side*

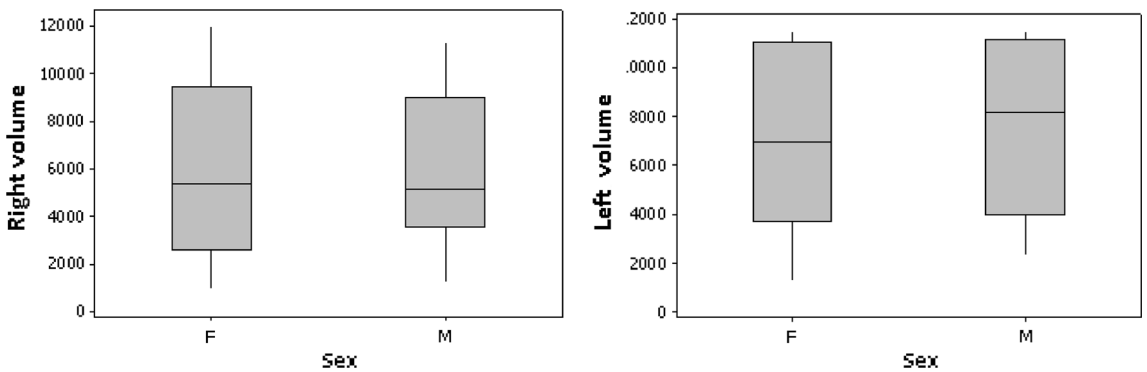


**Fig. 5** *Scatter plot* to the volume of the *right* and *left sides* by sex

**Table 2** Measures position and volume dispersion by sex and result of the comparison between groups (Mann–Whitney)

| Sex | Variables | *N* | Average | ±SD | Minimum | Median | Maximum | *P* value |
|---|---|---|---|---|---|---|---|---|
| F | Right volume | 27 | 6096.12 | 3637.49 | 929.75 | 5376.00 | 11,992.50 | 0.9229 |
| | Left volume | 27 | 7068.28 | 3726.61 | 1268.00 | 6945.00 | 11,455.50 | 0.6131 |
| M | Right volume | 20 | 6092.73 | 3376.34 | 1235.50 | 5125.00 | 11,327.00 | |
| | Left volume | 20 | 7419.60 | 3452.92 | 2286.00 | 8170.75 | 11,471.50 | |

Volumes (mm3)

*SD* standard deviation

**Table 3** Position and dispersion measures of the right volume for classification and result of the comparison between groups (Kruskal–Wallis)

| Right | *N* | % | Average | ±SD | Minimum | Median | Maximum | *P* value* |
|---|---|---|---|---|---|---|---|---|
| Conchal | 1 | 2.12 | 929.75 | – | 929.75 | 929.75 | 929.75 | 0.0002 |
| Pre-sellar | 6 | 12.76 | 2403.42 | 1119.52 | 1235.50 | 2229.00 | 4009.50 | |
| Post-sellar | 29 | 61.70 | 7768.24 | 3095.91 | 1072.50 | 7851.00 | 11,992.50 | |
| Sellar | 11 | 23.40 | 4165.50 | 2353.28 | 1060.00 | 3781.50 | 8343.00 | |

Volumes (mm3)

*SD* standard deviation

* *P* value disregarding conchal categories

**Table 4** Position and dispersion measures left for classification and result of the comparison between groups (Mann–Whitney)

| Left | *N* | % | Average | ±SD | Minimum | Median | Maximum | *P* value* |
|---|---|---|---|---|---|---|---|---|
| Conchal | 1 | 2.12 | 1268.00 | 1268.00 | 1268.00 | 1268.00 | 1268.00 | 0.0002 |
| Pre-sellar | 2 | 4.25 | 3798.75 | 1456.99 | 2768.50 | 3798.75 | 4829.00 | |
| Post-sellar | 31 | 65.95 | 8750.06 | 3146.39 | 2697.00 | 11,004.00 | 11,471.50 | |
| Sellar | 13 | 27.65 | 4547.54 | 2339.04 | 2178.50 | 4191.50 | 9664.50 | |

Volumes (mm3)

*SD* standard deviation

* *P* value disregarding conchal and pre-sellar categories

## Discussion

It is important to understand the internal anatomy of the sphenoid sinus due to its unique localization at the center of the skull, with surrounding structures of indisputable importance, and find out these anatomical relationships in its internal walls. Its asymmetry is due to the fact that the septum separating the right from the left side is curved and irregular. In our results, the sinus on the left side was slightly voluminous than the one on the right side. Some studies showed that sinuses have, on average, a volume of 9375 $mm^3$ until the first year of age, reaching 7820 $mm^3$ in adults [1–4]. In this study, approximate measurements were found, with volumes of the sphenoid sinuses reaching 6000 $mm^3$ on the right side and 7000 $mm^3$ on the left side in adults.

The sphenoid is considered the most inaccessible part of the face, being enclosed within the sphenoid bone and closely related to numerous vital neural and vascular structures. This inner localization can be a complicating factor for the success of the surgery [3]. The advent of functional endoscopic surgery and modern imaging techniques has allowed the sinus to be more frequently accessed not only for treatment of diseases, but also as a path towards the pituitary gland. Therefore, studies in the literature have confirmed the importance of knowing the anatomy of the sphenoid sinus. With the past developments in endoscopic surgery, the knowledge about the anatomy of paranasal sinuses has become crucial for the surgeons. This technique proved to be safe and effective for the treatment of pituitary adenomas, despite the complications related to internal carotid artery [2, 3, 7]. The variations in the paranasal sinuses should be carefully evaluated in each patient. The data obtained in the present study can prevent complications that rhinologists may face during endoscopic surgical procedures. One of our objectives was to raise the importance of anatomical knowledge to achieve greater

security in procedures involving paranasal sinuses and major related structures. Because the anatomical diversity of vital structures adjacent to the sphenoid sinus may complicate the functional endoscopic surgery, the knowledge of both size and extent of pneumatization of the sphenoid sinus is an important condition for performing a surgical treatment accordingly [13, 14, 16]. Therefore, a method helping this classification would be important in the diagnosis, since categorization often becomes difficult by only using the CT technique because of the shades of gray in the image.

In our methodology, we present a 3D model with color using manual segmentations in CT scans. Manual segmentation provides higher precision, but requirements more user interaction, due to strictly manual interaction [22]. The user has to go through around the images, slice by slice, to extract the outlines of the target structure and can make editing, but soft tissues are more difficult to segment due to no-homogeneous contrast [22], becoming the segmentation difficult and sometimes even impossible. So far, we chose not to include the surrounding structures in this work.

The software allows a 3D multi-orientation view and can capture the anatomical features of sinus accurately. Calculated volume can be shown separately. The application of 3D planning enables the surgeon has an accurate design of the anatomic fragment. A pathological variation of sinus anatomy, which could affect the volume, shape, or wall thickness, can be taken into account by the geometry of the 3D model [5, 10, 21, 28, 29]. 3D dimensionality improved hand–eye coordination, better tissue understanding and decreased learning curves [8]. For precise medical applications, manual segmentation will give the best results. However, a 3D model from airway cavity segmentation tended to have more inner fusion structures due to its nature (air, bone and mucosa) [15] and the septum edge definition tends to be poor.

Oliveira et al. [20] studied 25 men and 25 women examined by CT with 3D reconstruction and computer graphic applications. It was observed that men have apparently greater variation in both area and volume than women, on average. The significant difference found between the mean values of male and female groups made it possible to state that the method might be used for evaluation of sexual dimorphism, although our results showed no significant differences between gender and volume of the sinuses. Yonetsu et al. [31] reported that there were no difference in volume aeration between men and women, which is in agreement with our results. Anusha et al. [2] reported the prevalence of types of sinuses in a study with 279 patients, with sella being the most frequent type (93 %), followed by 6.7 % of pre-sellar and 0.3 % of conchal. In the present study, we found more post-sellar types, followed by sellar. Dias et al. [9] found sellar, post-sellar and pre-sella types in 54.45, 39.11 and 6.44 % of the cases, a finding diverging from our results. Mamatha et al. [18] found pneumatization in the majority of the patients with sellar type (55 %), whereas 5 patients had pre-sellar and 4 had post-sellar types. Seddighi et al. [24] studied the degree of pneumatization in a sample with 64 adult patients diagnosed with pituitary adenomas, in which 34 cases of sellar type (59.4 %), 10 cases of pre-sellar type (15.6 %) and 16 cases of conchal type (25 %) were observed. Tomovic et al. [26] found 1.8 % cases of conchal type, 7.3 % of pre-sellar type, 47.6 % of sellar type and 43.3 % of post-sellar type. Again, this higher incidence of sellar type in the majority of the cases does not agree with the results obtained in our study, in which the post-sellar type prevailed. The frequency rates of the types vary between several studies, which may be a result of diverse study techniques, the type of classification used and study sample size. A surgical implication of the post-sellar pneumatization of the sphenoid sinus is a possible penetration of the posterior wall of the sphenoid, with resultant cerebrospinal fluid leak [11].

The volume of the cavity in the paranasal sinuses is not only the simplest, but also the most important index for paranasal sinus evaluation [21]. We evaluated volume and anatomy shape (type of pneumatization of the sphenoid sinus) since identical shapes can present different volumes. Our study found statistically significant differences between the volume on the right and left sides of the same sinus (Figs. 6, 7).

Park et al. [21] reported that paranasal sinuses continue to expand in all directions as the development of the nasal cavity and other facial structures occurs between 1 and 7 years old. The pneumatization of the paranasal sinuses is almost complete between 12 and 14 years old, when the individual reached the growth proportions. Yonetsu et al. [31] found that the aeration of the sphenoid sinus is completed in 93 % of the population evaluated until the third decade of life. After the fourth decade of life, the aeration

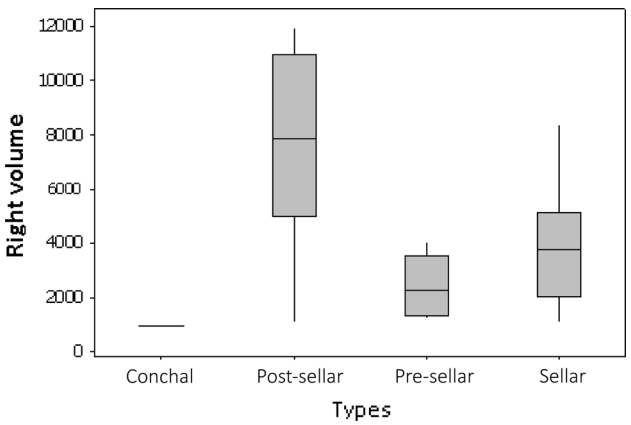


**Fig. 6** *Scatter plot* to the volume of the *right side* between groups

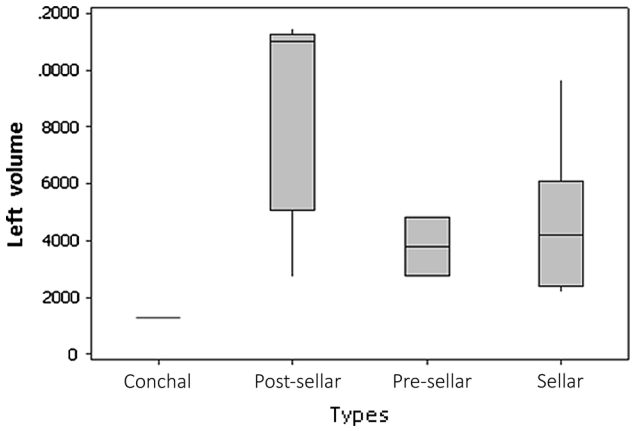


**Fig. 7** *Scatter plot* to the volume of the *left side* between groups

volume of the sphenoid sinus begins to decline until reaching two-third of its maximum level in the seventh decade of life. In the present study, however, there was no correlation between volume of the sinuses and age group. Stokovic et al. [25] warned that the tomographic and radiographic techniques may not be able to show all the required elements to cause an iatrogenic injury. The authors suggest that factors such as type of sinus and its basic dimensions (i.e. height, width and length) can help predict the risk of accidental injury. In this study, it was possible to facilitate the classification of the sphenoid sinus using 3D images to estimate precisely the volume of the entire structure.

## Conclusions

The post-sellar type was found to be more prevalent, followed by the sellar type. According to the methodology used, it can be concluded that 3D reconstruction proved to be a good method for categorizing the sphenoid sinus, improving its anatomical knowledge. The volume of the sphenoid sinus was influenced by neither gender nor age ($P > 0.005$). There are differences in the volumes of the sphenoid sinuses in the right and left sides, including their anatomical classification. We believe that it is important to carry out complementary studies into this field to prove the relationship of sinus volume with gender and age and underscore the significance of replicating our findings on larger samples.

### Compliance with ethical standards

**Conflict of interest** All the authors have made significant contributions to this work, with all co-authors approving the final version of this article and agreeing with its submission for publication. This study has not been published elsewhere, nor is currently being considered for publication in another journal. All the authors have no conflict of interest regarding the production of this article.

## References

1. Anusha B, Baharudin A, Philip R, Harvinder S, Shaffie BM (2014) Anatomical variations of the sphenoid sinus and its adjacent structures: a review of existing literature. Surg Radiol Anat 36:419–427. doi:10.1007/s00276-013-1214-1
2. Anusha B, Baharudin A, Philip R, Harvinder S, Shaffie BM, Ramiza RR (2015) Anatomical variants of surgically important landmarks in the sphenoid sinus: a radiologic study in Southeast Asian patients. Surg Radiol Anat 37:1183–1190. doi:10.1007/s00276-015-1494-8
3. Budu V, Mogoanta CA, Fanuta B, Bulescu I (2013) The anatomical relations of the sphenoid sinus and their implications in sphenoid endoscopic surgery. Rom J Morphol Embryol 54:13–16
4. Burke MC, Taheri R, Bhojwani R, Singh A (2015) A practical approach to the imaging interpretation of sphenoid sinus pathology. Curr Probl Diagn Radiol 44:360–370. doi:10.1067/j.cpradiol.2015.02.002
5. Cevidanes LH, Gomes LR, Jung BT, Gomes MR, Ruellas AC, Goncalves JR, Schilling J, Styner M, Nguyen T, Kapila S, Paniagua B (2015) 3D superimposition and understanding temporomandibular joint arthritis. Orthod Craniofac Res 18(Suppl 1):18–28. doi:10.1111/ocr.12070
6. Cevidanes LH, Tucker S, Styner M, Kim H, Chapuis J, Reyes M, Proffit W, Turvey T, Jaskolka M (2010) Three-dimensional surgical simulation. Am J Orthod Dentofac Orthop 138:361–371. doi:10.1016/j.ajodo.2009.08.026
7. Chone CT, Sampaio MH, Sakano E, Paschoal JR, Garnes HM, Queiroz L, Vargas AA, Fernandes YB, Honorato DC, Fabbro MD, Guizoni H, Tedeschi H (2014) Endoscopic endonasal transsphenoidal resection of pituitary adenomas: preliminary evaluation of consecutive cases. Braz J Otorhinolaryngol 80:146–151
8. Costa AL, Yasuda CL, Appenzeller S, Lopes SL, Cendes F (2008) Comparison of conventional MRI and 3D reconstruction model for evaluation of temporomandibular joint. Surg Radiol Anat 30:663–667. doi:10.1007/s00276-008-0400-z
9. Dias PCJ, Albernaz PLM, Yamashida HK (2004) Relação anatômica do nervo óptico com o seio esfenoidal: estudo por tomografia computadorizada. Rev Bras Otorrinolaringol 70:651–657
10. Gocmez C, Goya C, Hamidi C, Teke M, Hattapoglu S, Kamasak K (2014) Evaluation of the surgical anatomy of sphenoid ostium with 3D computed tomography. Surg Radiol Anat 36:783–788. doi:10.1007/s00276-013-1245-7
11. Hamid O, El Fiky L, Hassan O, Kotb A, El Fiky S (2008) Anatomic variations of the sphenoid sinus and their impact on trans-sphenoid pituitary surgery. Skull Base 18:9–15. doi:10.1055/s-2007-992764
12. Hammer G, Radberg C (1961) The sphenoidal sinus. An anatomical and roentgenologic study with reference to transsphenoid hypophysectomy. Acta Radiol 56:401–422
13. Kaplanoglu H, Kaplanoglu V, Dilli A, Toprak U, Hekimoglu B (2013) An analysis of the anatomic variations of the paranasal sinuses and ethmoid roof using computed tomography. Eurasian J Med 45:115–125. doi:10.5152/eajm.2013.23
14. Kazkayasi M, Karadeniz Y, Arikan OK (2005) Anatomic variations of the sphenoid sinus on computed tomography. Rhinology 43:109–114
15. Kiraly AP, Higgins WE, McLennan G, Hoffman EA, Reinhardt JM (2002) Three-dimensional human airway segmentation methods for clinical virtual bronchoscopy. Acad Radiol 9:1153–1168

16. Lazaridis N, Natsis K, Koebke J, Themelis C (2010) Nasal, sellar, and sphenoid sinus measurements in relation to pituitary surgery. Clin Anat 23:629–636. doi:10.1002/ca.20984
17. Levine H (1978) The sphenoid sinus, the neglected nasal sinus. Arch Otolaryngol 104:585–587
18. Mamatha HS, Prasanna LC, Saraswathi G (2010) Variations of sphenoid sinus and their impact on related neurovascular structures. Curr Neurobiol 1:121–124
19. Miranda CMNRD, Maranhão CPDM, Arraes FMNR, Padilha IG, Farias LDPGD, Jatobá MSDA, Andrade ACMD, Padilha BG (2011) Variações anatômicas das cavidades paranasais à tomografia computadorizada multislice: o que procurar? Radiol Bras 44:256–262
20. Oliveira JX, Perrella A, Santos KCP, Sales MAO, Cavalcanti MGP (2009) Accuracy assessment of human sphenoidal sinus volume and area measure and its relationship with sexual dimorphism using the 3D-CT. Rev Inst Ciênc Saúde 27:390–393
21. Park IH, Song JS, Choi H, Kim TH, Hoon S, Lee SH, Lee HM (2010) Volumetric study in the development of paranasal sinuses by CT imaging in Asian: a pilot study. Int J Pediatr Otorhinolaryngol 74:1347–1350. doi:10.1016/j.ijporl.2010.08.018
22. Pirner S, Tingelhoff K, Wagner I, Westphal R, Rilk M, Wahl FM, Bootz F, Eichhorn KW (2009) CT-based manual segmentation and evaluation of paranasal sinuses. Eur Arch Otorhinolaryngol 266:507–518. doi:10.1007/s00405-008-0777-7
23. Rahmati A, Ghafari R, AnjomShoa M (2016) Normal variations of sphenoid sinus and the adjacent structures detected in cone beam computed tomography. J Dent (Shiraz) 17:32–37
24. Seddighi AS, Seddighi A, Mellati O, Ghorbani J, Raad N, Soleimani MM (2014) Sphenoid sinus: anatomic variations and their importance in trans-sphenoid surgery. Int Clin Neurosci J 1:31–34
25. Stokovic N, Trkulja V, Dumic-Cule I, Cukovic-Bagic I, Lauc T, Vukicevic S, Grgurevic L (2016) Sphenoid sinus types, dimensions and relationship with surrounding structures. Ann Anat 203:69–76. doi:10.1016/j.aanat.2015.02.013
26. Tomovic S, Esmaeili A, Chan NJ, Shukla PA, Choudhry OJ, Liu JK, Eloy JA (2013) High-resolution computed tomography analysis of variations of the sphenoid sinus. J Neurol Surg B Skull Base 74:82–90. doi:10.1055/s-0033-1333619
27. Wang S, Zhang J, Xue L, Wei L, Xi Z, Wang R (2015) Anatomy and CT reconstruction of the anterior area of sphenoid sinus. Int J Clin Exp Med 8:5217–5226
28. Wang SS, Xue L, Jing JJ, Wang RM (2012) Virtual reality surgical anatomy of the sphenoid sinus and adjacent structures by the transnasal approach. J Craniomaxillofac Surg 40:494–499. doi:10.1016/j.jcms.2011.08.008
29. Yasuda CL, Costa AL, Franca M Jr, Pereira FR, Tedeschi H, de Oliveira E, Cendes F (2010) Postcraniotomy temporalis muscle atrophy: a clinical, magnetic resonance imaging volumetry and electromyographic investigation. J Orofac Pain 24:391–397
30. Yilmaz N, Kose E, Dedeoglu N, Colak C, Ozbag D, Durak MA (2016) Detailed anatomical analysis of the sphenoid sinus and sphenoid sinus ostium by cone-beam computed tomography. J Craniofac Surg. doi:10.1097/SCS.0000000000002861
31. Yonetsu K, Watanabe M, Nakamura T (2000) Age-related expansion and reduction in aeration of the sphenoid sinus: volume assessment by helical CT scanning. AJNR Am J Neuroradiol 21:179–182
32. Yushkevich PA, Piven J, Hazlett HC, Smith RG, Ho S, Gee JC, Gerig G (2006) User-guided 3D active contour segmentation of anatomical structures: significantly improved efficiency and reliability. Neuroimage 31:1116–1128. doi:10.1016/j.neuroimage.2006.01.015